

Algorithm for Fast Monoexponential Fitting Based on Auto-Regression on Linear Operations (ARLO) of Data

Mengchao Pei,^{1,2} Thanh D. Nguyen,³ Nanda D. Thimmappa,³ Carlo Salustri,^{3,4} Fang Dong,¹ Mitch A. Cooper,³ Jianqi Li,¹ Martin R. Prince,³ and Yi Wang^{3,5*}

Purpose: To develop a fast and accurate monoexponential fitting algorithm based on Auto-Regression on Linear Operations (ARLO) of data, and to validate its accuracy and computational speed by comparing it with the conventional Levenberg-Marquardt (LM) and Log-Linear (LL) algorithms.

Methods: ARLO, LM, and LL performances for T₂^{*} mapping were evaluated in simulation and in vivo imaging of liver (n = 15) and myocardial (n = 1) iron overload patients and the brain (two healthy volunteers).

Results: In simulations, ARLO consistently delivered accuracy similar to LM and significantly superior to LL. In in vivo mapping of T₂^{*} values, ARLO showed excellent agreement with LM, while LL showed only limited agreements with ARLO and LM. Compared with LM and LL in the liver, ARLO was 125 and 8 times faster using our Matlab implementations, and 156 and 13 times faster using our C++ implementations. In C++ implementations, ARLO reduced the online whole-brain processing time from 9 min 15 s of LM and 35 s of LL to 2.7 s, providing T₂^{*} maps approximately in real time.

Conclusion: Due to comparable accuracy and significantly higher speed, ARLO can be considered as a valid alternative to the conventional LM algorithm for online T₂^{*} mapping.

Magn Reson Med 73:843–850, 2015. © 2014 Wiley Periodicals, Inc.

Key words: T₂^{*} mapping; autoregression; Levenberg-Marquardt; Log-Linear; iron overload

INTRODUCTION

The use of monoexponential fitting of the MR signal has been central to the development of many quantitative MR methods for mapping tissue properties. For example, the rate of signal decay in gradient echo (GRE) MRI ($R_2^* = 1/$

T_2^*), which is normally determined by fitting the GRE signal amplitudes recorded at various echo times (TEs), has been widely used to quantify iron deposition in the brain (1–3), heart (4,5), and liver (6–10). Currently, the nonlinear least squares based Levenberg-Marquardt (LM) (4,6,7,10) and the linear Log-Linear (LL) (8,11,12) are the most commonly used methods for monoexponential fitting. The iterative LM is generally regarded as more accurate but computationally more expensive than the noniterative LL (13). Moreover, LM requires a good initial guess to avoid convergence to local minima. LL, which simply performs a linear fit of the decay curve after a log transformation, is much faster and has been widely implemented by scanner vendors to provide quick T₂^{*} maps. Unfortunately, it is known to be quite sensitive to noise and may not work well when T₂^{*} is short (13).

In this study, we report on a novel alternative method for calculating T₂^{*}, based on applying a linear operation (e.g., integration) on the exponential decay curve and estimating T₂^{*} by means of a maximum-likelihood fit of an autoregressive model. We named our method Auto Regression on Linear Operations (ARLO) on MRI data. We assessed ARLO's accuracy and speed by comparing its performance with the ones of LM and LL in mapping T₂^{*} in computer simulations and in in vivo MRI of both healthy volunteers and iron-overloaded patients.

METHODS

The ARLO Algorithm

In the absence of noise, the measured GRE signal magnitude $m(t)$, acquired at echo time t can be expressed by a monoexponential decay:

$$m(t) = M_0 \exp(-t/T_2^*) \quad [1]$$

where M_0 is the proton density (weighted by T₁, RF receiver coil sensitivity and other sequence parameters). Integrating $m(t)$ over J consecutive echoes after the i th one (at echo time t_i) yields the following integrated signal:

$$s_i = \int_{t_i}^{t_{i+J}} m(t) dt = T_2^* [m(t_i) - m(t_{i+J})] \equiv T_2^* \delta_i \quad [2]$$

where N is the number of measured data points, $\delta_i = m(t_i) - m(t_{i+J})$, and $i = 1, \dots, N - J$. For simplicity, we consider the case $J = 2$ with an equidistant echo interval ΔTE , in which case Eq. [2] becomes:

$$s_i = T_2^* [m(t_i) - m(t_{i+2})] \quad [3]$$

¹Shanghai Key Laboratory of Magnetic Resonance and Department of Physics, East China Normal University, Shanghai, China.

²Yifu Inc, Jiaxing, Zhejiang Province, China.

³Radiology, Weill Cornell Medical College, New York, New York, USA.

⁴Institute of Cognitive Sciences and Technologies (CNR), Rome, Italy.

⁵Department of Biomedical Engineering, Kyung Hee University, Seoul, South Korea.

Grant sponsor: The National Natural Science Foundation of China; Grant number: 81271533.

*Correspondence to: Yi Wang, Ph.D., 515 East 71st Street, New York, NY, 10065. E-mail: yiwang@med.cornell.edu

Additional Supporting Information may be found in the online version of this article.

Received 22 May 2013; revised 30 December 2013; accepted 30 December 2013

DOI 10.1002/mrm.25137

Published online 24 March 2014 in Wiley Online Library (wileyonlinelibrary.com).

© 2014 Wiley Periodicals, Inc.

The integral in Eq. [2] can be computed numerically using the Simpson's rule to the fourth order accuracy (14):

$$s_i \cong \frac{\Delta TE}{3} [m(t_i) + 4m(t_{i+1}) + m(t_{i+2})] \quad [4]$$

By equating the right-hand sides of Eqs. [3] and [4] and then solving for $m(t_{i+2})$, we obtain the following linear recurrence relation for the signal $m(t_{i+2})$:

$$m(t_{i+2}) = -\frac{\frac{4\Delta TE}{3}}{T_2^* + \frac{\Delta TE}{3}} m(t_{i+1}) + \frac{T_2^* - \frac{\Delta TE}{3}}{T_2^* + \frac{\Delta TE}{3}} m(t_i) \quad [5]$$

So far we have considered the case of a noiseless signal, whereas in reality the measured magnitude signal $m(t_i)$ of Eq. [1] is always contaminated by some noise $n(t_i)$. When the signal-to-noise ratio (SNR) ≥ 3 , this noise is well approximated by a Gaussian distribution (15,16), whose mean varies with the signal magnitude, thus introducing a signal-dependent bias in each data point (16), which can be corrected for if the noise statistics are known. The noise in the corrected signal can then be approximated as zero-mean, independent and identically distributed (i.i.d.) Gaussian noise, in which case the measured signal $m(t_{i+2})$ follows an autoregressive (AR) time series model of order 2:

$$m(t_{i+2}) = -\frac{\frac{4\Delta TE}{3}}{T_2^* + \frac{\Delta TE}{3}} m(t_{i+1}) + \frac{T_2^* - \frac{\Delta TE}{3}}{T_2^* + \frac{\Delta TE}{3}} m(t_i) + n(t_{i+2}), \quad [6]$$

The AR model coefficients can be obtained as a maximum-likelihood estimate by minimizing the following cost function (17):

$$\min_{T_2^*} \sum_{i=1}^{N-2} \left(m(t_{i+2}) + \frac{4\Delta TE/3}{T_2^* + \Delta TE/3} m(t_{i+1}) - \frac{T_2^* - \Delta TE/3}{T_2^* + \Delta TE/3} m(t_i) \right)^2 \quad [7]$$

Thus, T_2^* can be obtained by the following minimizer:

$$T_2^* = \arg \min_{T_2^*} \frac{1}{(T_2^* + \Delta TE/3)^2} \sum_{i=1}^{N-2} (s_i - T_2^* \delta_i)^2 \quad [8]$$

whose analytical solution gives us the value of T_2^* :

$$T_2^* = \frac{\sum_{i=0}^{N-2} s_i^2 + \Delta TE/3 \sum_{i=0}^{N-2} s_i \delta_i}{\Delta TE/3 \sum_{i=0}^{N-2} s_i^2 + \sum_{i=0}^{N-2} s_i \delta_i} \quad [9]$$

Algorithm Implementation

ARLO was implemented according to Eq. [9] on multiecho GRE data with equidistant echo spacing. For comparison, the conventional LM and LL methods were also implemented as described in the literature (4,6–8,10–12). The initial guess of T_2^* in LM was 5 ms. Two strategies were used simultaneously to mitigate the detrimental effect of Rician noise, following a central chi statistic (16), in the magnitude image obtained with sum-of-squares reconstruction: (i) Data truncation (4,7,8,10,18,19), in which only the first consecutive M data points were kept ($M \geq 3$), whose values were above a preset threshold (mean plus twice the standard deviation of the noise measured in a background

region of the magnitude image); (ii) Rician noise bias correction applied to the remaining data points, using a lookup table method (16,20). Data truncation and noise bias correction were applied to all three algorithms.

All simulations, as well as in vivo liver GRE data, were processed using Matlab 7 R2010a (Mathworks, Natick, MA) on a Windows 7 desktop computer (Intel Core i7 2.8 GHz processor, 18 GB memory). In vivo brain and cardiac data were processed using custom C++ implementations of all three algorithms on the host computer of a GE HDxt scanner running 15.0 software (General Electric, Milwaukee, WI, USA).

Simulation Study

To assess the accuracies of ARLO, LM, and LL, we performed computer simulations using known T_2^* values. The effects of T_2^* (which affects the number of data points used for the fit after data truncation), of SNR, and of the number of receiver coils (which introduces different noise biasing conditions) were considered. More specifically, T_2^* was set to 1.5, 10, and 20 ms, SNR was varied from 20 to 100, and the number of receiver coils was set to 1 and 8, while assuming 16 equidistant echoes in the 1.3–23.3 ms range (same as the one used in our liver protocol). The relative T_2^* bias was computed as $[\text{mean}(T_2^*_{\text{estimated}}) - T_2^*_{\text{true}}] / T_2^*_{\text{true}} \times 100\%$.

To model Rician noise, a zero-mean i.i.d. Gaussian noise (with a standard deviation σ_0) was added to the real and imaginary channels of each receiver coil and the T_2^* decay curve was computed as the square root of the sum-of-squares of the signals from all receivers. SNR was defined as M_0/σ_0 (16,21), where M_0 is the preset signal amplitude at $TE=0$. Ten thousand trials were repeated for each combination of SNR, T_2^* value and number of receivers to estimate the mean and standard deviation of T_2^* errors.

MRI Study

This retrospective study was approved by the local Institutional Review Board. Liver MR images were obtained from 15 patients (6 men and 9 women, mean age = 27 years \pm 10, of whom 12 had known hemochromatosis and 3 had β thalassemia) on a 1.5 Tesla (T) scanner (General Electric, Milwaukee, WI), equipped with an eight-channel body phased-array coil. A breath-hold two-dimensional (2D) GRE sequence was used with the following imaging parameters: repetition time (TR) = 27.4 ms, echo time (TE) = 1.3 to 23.3 ms (16 uniformly spaced echoes with echo spacing = 1.47 ms), flip angle = 20°, field of view (FOV) = 48 cm, matrix size = 256 \times 256, slice thickness = 10 mm with a 5 mm gap, four transversal slices. Parallel imaging was not used. To further demonstrate the generality of the proposed method, multiecho GRE data were also acquired at 3T from the brains of two healthy volunteers (isotropic 3D acquisition, 7 and 12 echoes with echo spacing = 6.5 ms and 4.1 ms, respectively, flip angle = 20°, FOV = 23 cm, matrix size = 328 \times 328 interpolated to 512 \times 512, phase FOV factor = 0.75, partial echo factor = 0.75, slice thickness = 0.7 mm, 206 axial slices) and at 1.5T from the heart of one patient with myocardial iron overload (2D acquisition, TR = 19.0 ms, TE = 2.8 to 16.8 ms, 8 echoes with echo spacing = 2.0 ms, flip

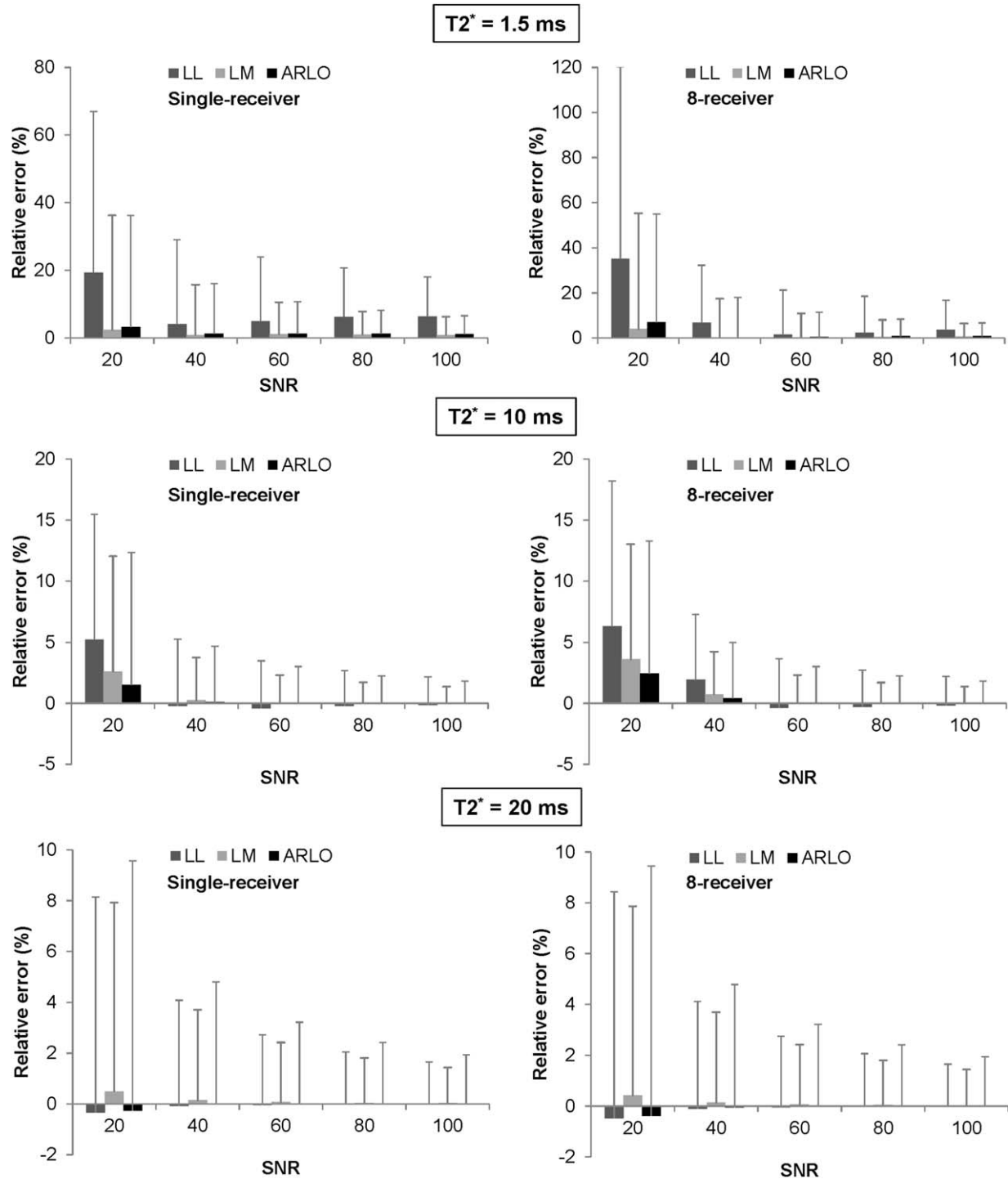


FIG. 1. Comparison of mean and standard deviation of relative T_2^* error as a function of SNR obtained with log-linear (LL), Levenberg-Marquardt (LM), and ARLO methods, using numerical simulations for $T_2^* = 1.5, 10$, and 20 ms and number of coil receivers = 1 and 8.

angle = 35° , FOV = 36 cm, matrix size = 192×128 , slice thickness = 8 mm, 4 short-axis slices). All multiecho GRE data were acquired with monopolar readout gradients.

Liver regions-of-interest (ROIs) were first manually traced by an experienced radiologist on the first echo image and then eroded by two pixels to remove partial voxels near the liver/blood and liver/fat interfaces. Liver T_2^* maps obtained with ARLO, LM, and LL were compared on a mean ROI basis in all subjects and on a voxel

basis in one subject. Liver SNR was calculated for each subject from a middle slice by dividing the mean liver signal measured within the ROI at the first TE by the noise standard deviation in the real/imaginary channel, estimated from the background noise statistics for an eight-channel phased array coil (16). For brain images, skull stripping was performed before T_2^* fitting. The basal ganglia in the brain and the myocardium were manually traced and processed for T_2^* comparison

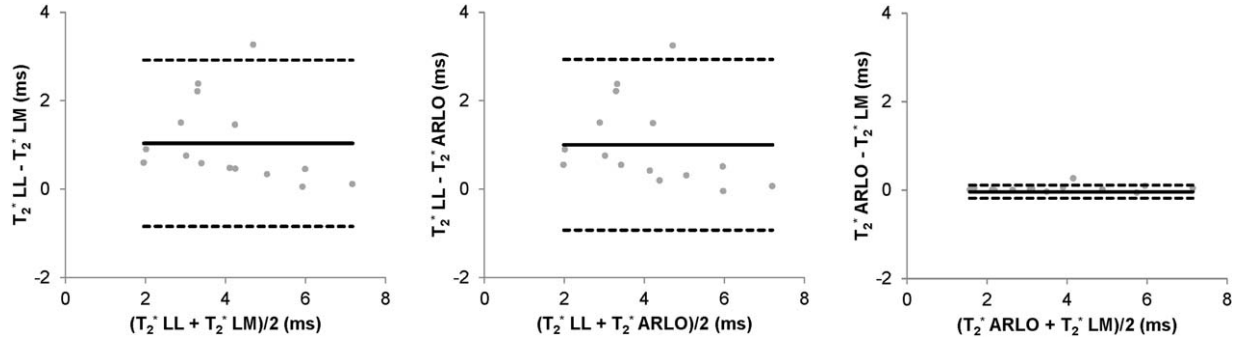


FIG. 2. Bland-Altman plots of liver T_2^* values (in ms) obtained by mean ROI analysis over 15 liver patients at 1.5T using the conventional log-linear (LL) and Levenberg-Marquardt (LM) methods and the proposed ARLO method (also see linear regression plots in the Supporting Information, which is available online).

analysis. Statistical analyses included linear regression, Bland-Altman analysis and two-tailed paired sample *t*-test applied to liver, brain and heart data.

RESULTS

The results of our simulation are shown in Figure 1. ARLO and LM delivered lower bias (higher accuracy) and smaller standard deviation (higher precision) than LL over the investigated range of SNR (20–100) and for the chosen number of receivers (1 and 8), and for T_2^* between 1.5 and 10 ms. Compared with LM at a very short T_2^* of 1.5 ms, ARLO had a slightly larger bias and a slightly smaller standard deviation. At $T_2^* = 20$ ms, ARLO still yielded the lowest bias, although with a slightly larger standard deviation. The relative T_2^* biases of ARLO and LM remained consistently within 4%. However, the bias delivered by LL resulted in greater sensitivity to T_2^* , SNR and the number of receivers (5.2–13.9% range), and increased sharply for short T_2^* and a high number of receiver coils. Compared with LM, ARLO provided slightly lower biases and slightly higher standard deviations, although these differences were virtually negligible.

Figure 2 compares the mean ROI analyses obtained with the three fitting methods in the iron-overloaded liver ($n = 15$). The range as well as the mean and standard deviation of T_2^* values (in ms), averaged over all patients were [2.3–7.2, 4.6 ± 1.4] for LL, [1.6–7.1, 3.6 ± 1.7] for LM, and [1.6–7.2, 3.6 ± 1.7] for ARLO. LM showed limited correlation and agreement with both LM ($R^2 = 0.699$) and ARLO ($R^2 = 0.688$), while ARLO agreed well with LM ($R^2 = 0.998$, slope of regression line = 1.007, -0.03 ms bias and -0.18 – 0.11 ms confidence interval) ($P < 0.01$). The average liver SNR was 87 ± 18 . The T_2^* fitting time in Matlab for 4 slices averaged over 15 subjects was 87.6 ± 28.9 s for LM and 5.8 ± 1.7 s for LL, which decreased to 0.7 ± 0.2 s for the proposed ARLO method. On a per-voxel basis, the fitting time was 8.81 ± 1.00 , 0.57 ± 0.04 , and 0.07 ± 0.02 ms for LM, LL, and ARLO, respectively, representing a 125 and 8 times gain in computational speed by ARLO.

Figure 3 shows an example of liver source images, the derived T_2^* maps, and voxel-based comparisons of the three methods using linear regression and Bland-Altman plots within one subject. Range, mean, and standard deviation of T_2^* values (in ms) within the liver were

[2.1–15.3, 4.0 ± 1.3] for LL, [2.7–5.3, 3.7 ± 0.3] for LM, and [2.8–5.6, 3.8 ± 0.3] for ARLO. Similar to the mean ROI analysis (Fig. 2), LL had a rather poor linear correlation and limited agreement with both LM ($R^2 = 0.294$) and ARLO ($R^2 = 0.194$). Unlike LL, ARLO had instead an excellent linear correlation with LM ($R^2 = 0.946$, slope of regression line = 0.922) and a very narrow range of agreement (mean bias of -0.04 ms and -0.19 – 0.11 ms confidence interval) ($P < 0.01$).

Figure 4 shows a comparison of brain T_2^* maps obtained from a healthy volunteer at 3T. Figure 5 shows an example of cardiac T_2^* maps obtained from a patient with myocardial iron overload. Using LM as the reference method, T_2^* values obtained with ARLO in both the basal ganglia and the heart had a higher correlation ($R^2 = 0.95$ and 0.96 , respectively) and narrower limits of agreement than that obtained with LL ($R^2 = 0.89$ and 0.80 , respectively) (Figs. 4 and 5). On the average ($n = 2$), the processing time for the whole brain (approximately 11 million voxels) using our C++ implementations on a GE scanner was 35 s and 9 min 15 s for LL and LM, respectively, while ARLO took 2.7 s.

DISCUSSION

Our data demonstrate that ARLO is more robust against noise than LL in mapping T_2^* , while delivering an accuracy similar to LM. However, ARLO's most striking improvement over the other two methods is represented by its computational speed, as ARLO proved approximately 100 times faster than LM and 10 times faster than LL. This characteristic allowed us to obtain an accurate whole-organ T_2^* mapping in a very short time and our in vivo evaluation in healthy volunteers and iron-overloaded patients showed that ARLO delivers T_2^* maps very similar to those obtained with LM.

The processing speed advantage can be understood in terms of computational cost estimates. ARLO uses a single-variable linear regression with a computational cost $O(N)$, where N is the number of data points. LL uses a two-variable linear regression with a computational cost $O(6N)$. In LM, the number of iterations needed for solving the nonlinear least squares problem has a computational cost of $O(N^3)$. Thus, one expects ARLO to be faster than LL, and both ARLO and LL to be much faster than LM. Our experimental observations confirmed these predictions.

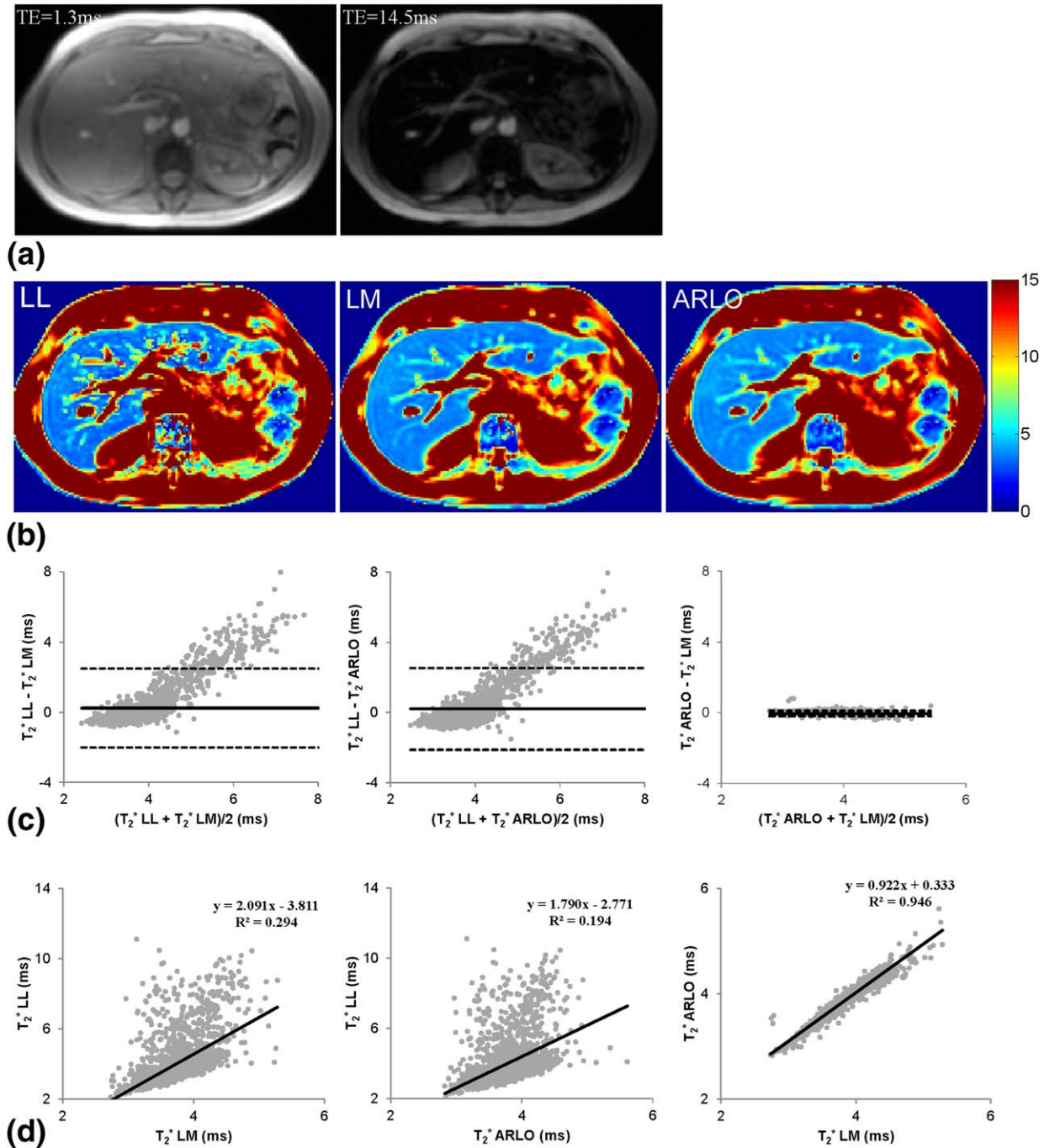


FIG. 3. Example of multiecho gradient echo source images (a) and derived T_2^* maps (in ms) (b) obtained from a patient with liver iron overload using log-linear (LL), Levenberg-Marquardt (LM), and ARLO algorithms. Note the increased noise in the map obtained with LL method. Bland-Altman plots and scatter plots (with linear regression lines) comparing liver T_2^* are shown in c and d, respectively. The total fitting time of four slices for LM, LL, and ARLO was 94, 8, and 0.9 s using our Matlab implementations and 313, 26, and 2 ms using our C++ implementations.

Noise propagation is a major cause of error in T_2^* mapping, particularly for iron-overloaded cases, where the short T_2^* leads to poor SNR. LL is very sensitive to noise, as its log operation amplifies noise effects (13). LM solves a nonlinear least squares problem and provides the optimal maximum likelihood estimate when noise is Gaussian (18). The maximum likelihood estimate for Rician noise has been previously derived elsewhere (20). However, minimizing nonlinear cost functions using iterative methods, such as LM, in the presence of noise is

prone to errors due to the need for an initial guess and to convergence issues as well as requires significant computational power. ARLO provides an effective linearization of the nonlinear estimation problem, therefore providing a near-optimal solution in significantly reduced processing time. Unlike LM, ARLO provides a closed-form solution and requires simple arithmetics to compute T_2^* from the multiecho data (Eq. [9]). As such, ARLO does not require an initial guess and is immune to convergence issues commonly associated with iterative

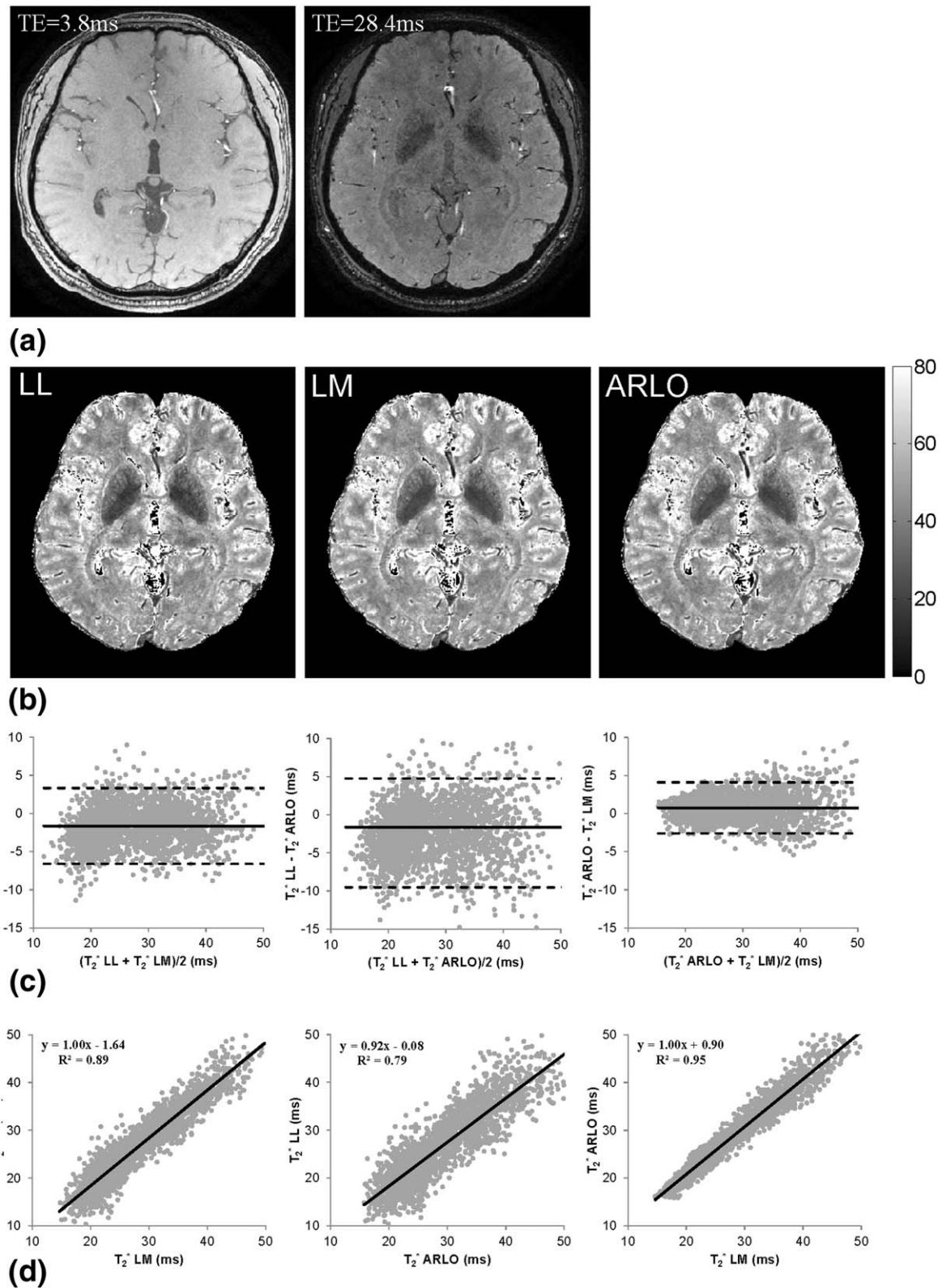


FIG. 4. Example of T2* weighted gradient echo images (a) and extracted brain T2* maps (in ms) (b) obtained from a healthy volunteer at 3T using log-linear (LL), Levenberg-Marquardt (LM), and ARLO algorithms. Note the reduced T2* in the basal ganglia due to iron storage in this area. Bland-Altman plots and scatter plots (with linear regression lines) comparing T2* in the basal ganglia are shown in c and d, respectively. The total fitting time of this whole brain 0.7 mm isotropic 3D data set with 12 echoes (using our C++ implementations on the host computer of a GE HDxt scanner) was 41 s and 10 min for LL and LM, respectively, while ARLO took only 3.4 s.

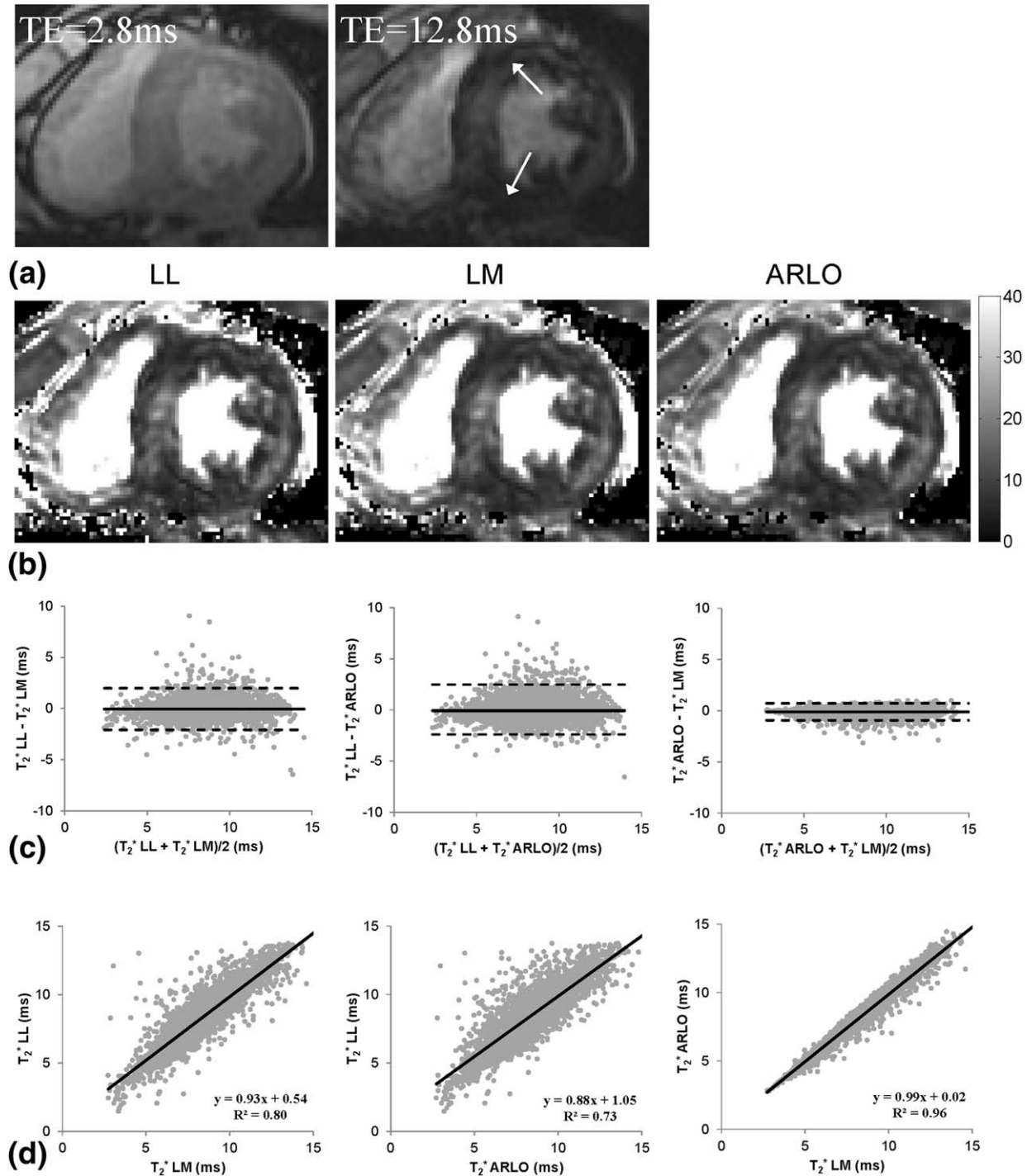


FIG. 5. Example of T_2^* weighted gradient echo images (a) and cardiac T_2^* maps (in ms) (b) obtained from a patient with myocardial iron overload at 1.5T using log-linear (LL), Levenberg-Marquardt (LM), and ARLO algorithms. Myocardial regions with markedly decreased T_2^* indicate the presence of iron (arrows). Bland-Altman plots and scatter plots (with linear regression lines) comparing myocardial T_2^* are shown in c and d, respectively. The C++ fitting time for the myocardium shown in this example was 4, 0.2, and 0.02 s for LM, LL, and ARLO, respectively.

methods such as LM. In this study, we used the well-known Simpson rule (Eq. [4]) to approximate the definite integral in Eq. [2]. This formula is derived from a quadratic approximation and provides a fourth order accuracy (14). By using computer simulations (data not shown), we found that this approximation provides much improved accuracy when compared with the fourth order approximation (i.e., using the trapezoidal rule), while

higher order approximations (e.g., cubic approximation using the 3/8 Simpson rule) yielded little benefit.

It is worth noticing that, in addition to integration, differentiation of Eq. [1] using the central difference method is an alternative way to generate a signal magnitude time series. Higher order approximations are also possible using more points, as for example the fourth order accuracy with five points (14). $1/T_2^*$ is obtained as the

maximum-likelihood estimate of the resulting AR model. In this study, we chose integration (Eq. [2]) over differentiation because it provides higher accuracy with large sampling intervals and low SNRs, in agreement with error analysis of numerical implementation of integration and differentiation (14). However, with higher SNRs and adequate sampling intervals, differentiation becomes as accurate as integration (results not shown).

The integration of the signal equation with an exponential factor uniquely generates a time series, an issue that has been well studied in signal processing. Accordingly, time series analysis techniques, including autoregression, can be applied on measured data. The exponential coefficient can be optimally determined by using the maximal likelihood estimation (17). This autoregression on linear operations approach can also be applied for determining exponential coefficients in other MRI experiments and other signals outside MRI. ARLO applications in other MRI studies include estimating the spin-spin relaxation time T_2 from data measured at various TEs, $m(t) = M_0 \exp(-t/T_2)$; estimating off-resonance field b and T_2^* from data measured at various TEs, $m(t) = M_0 \exp(-t(\frac{1}{T_2} + i\gamma b))$; estimating the diffusion coefficient D from data measured at various gradient b values, $m(t) = M_0 \exp(-Db)$; and estimating the spin-lattice relaxation time T_1 from data measured at various timing parameters, such as TR or TI, $m(t) = M_{z0} \exp(-t/T_1) + M_0(1 - \exp(-t/T_1))$. For the case of $\frac{1}{T_2} + i\gamma b$ estimation, complex data has to be used in linear regression. For the case of T_1 estimation, which usually requires fitting a three-parameter monoexponential model, a constant term may be needed in the linear regression. The ARLO approach may be modified to handle such constant offset, in addition to the noise baseline in the magnitude data obtained with a multiple-receiver coil to avoid bias (20).

It is important to note that while the ARLO algorithm proposed in this work (Eq. [9]) is only suited for monoexponential fitting, i.e., for a single chemical species, it can be generalized to handle multiexponential or multispectral T_2/T_2^* decay data when multiple tissue compartments and/or multiple chemical species occupy the same imaging voxel, as in the case of fat and water in-voxel coexistence in the liver. However, more sophisticated fitting algorithms have been developed recently to deal with these problems (9,22,23).

A potential limitation of the method implemented in this work is the minimum detectable T_2^* , which can be important for patients with severe iron overload. In our liver scans, we used a monopolar (instead of bipolar) readout gradient to avoid the time shift between even and odd echoes, resulting in an echo spacing of 1.5 ms. Furthermore, our ARLO implementation requires a minimum of three data points (compared with two by LM and LL). Our simulations indicate that these limitations in echo spacing and number of required data points result in a minimum detectable T_2^* of approximately 1.5 ms by ARLO. Further reducing both the first TE and the echo spacing is therefore critical for the detection of species with very short T_2^* (≤ 1.5 ms).

In conclusion, our proposed ARLO algorithm provides fast and accurate T_2^* maps and is, therefore, well-suited for whole-organ T_2^* mapping in iron overload diseases, besides showing potential also in other quantitative MRI

studies. ARLO can replace the LL algorithm for accurate online T_2^* mapping, and replace the LM algorithm for accurate fast analysis of exponential signal behaviors.

REFERENCES

1. Aquino D, Bizzi A, Grisoli M, Garavaglia B, Bruzzone MG, Nardocci N, Savoiardo M, Chiapparini L. Age-related iron deposition in the basal ganglia: quantitative analysis in healthy subjects. *Radiology* 2009;252:165–172.
2. Ropele S, Wattjes MP, Langkammer C, et al. Multicenter R_2^* mapping in the healthy brain. *Magn Reson Med* 2014;71:1103–1107.
3. Khalil M, Langkammer C, Ropele S, et al. Determinants of brain iron in multiple sclerosis: a quantitative 3T MRI study. *Neurology* 2011;77:1691–1697.
4. He T, Gatehouse PD, Smith GC, Mohiaddin RH, Pennell DJ, Firmin DN. Myocardial T_2^* measurements in iron-overloaded thalassemia: An in vivo study to investigate optimal methods of quantification. *Magn Reson Med* 2008;60:1082–1089.
5. Carpenter JP, He T, Kirk P, et al. On T_2^* magnetic resonance and cardiac iron. *Circulation* 2011;123:1519–1528.
6. Wood JC, Enriquez C, Ghugre N, Tyzka JM, Carson S, Nelson MD, Coates TD. MRI R_2 and R_2^* mapping accurately estimates hepatic iron concentration in transfusion-dependent thalassemia and sickle cell disease patients. *Blood* 2005;106:1460–1465.
7. Hankins JS, McCarville MB, Loeffler RB, Smeltzer MP, Onciu M, Hoffer FA, Li CS, Wang WC, Ware RE, Hillenbrand CM. R_2^* magnetic resonance imaging of the liver in patients with iron overload. *Blood* 2009;113:4853–4855.
8. Henninger B, Kremser C, Rauch S, Eder R, Zoller H, Finkenstedt A, Michaely HJ, Schocke M. Evaluation of MR imaging with T_1 and T_2^* mapping for the determination of hepatic iron overload. *Eur Radiol* 2012;22:2478–2486.
9. Taylor BA, Loeffler RB, Song R, McCarville MB, Hankins JS, Hillenbrand CM. Simultaneous field and R_2 mapping to quantify liver iron content using autoregressive moving average modeling. *J Magn Reson Imaging* 2012;35:1125–1132.
10. Langkammer C, Krebs N, Goessler W, Scheurer E, Ebner F, Yen K, Fazekas F, Ropele S. Quantitative MR imaging of brain iron: a post-mortem validation study. *Radiology* 2010;257:455–462.
11. Hoppe S, Quirbach S, Mamisch TC, Krause FG, Werlen S, Benneker LM. Axial T_2^* mapping in intervertebral discs: a new technique for assessment of intervertebral disc degeneration. *Eur Radiol* 2012;22:2013–2019.
12. Mamisch TC, Hughes T, Mosher TJ, Mueller C, Trattnig S, Boesch C, Welsch GH. T_2 star relaxation times for assessment of articular cartilage at 3 T: a feasibility study. *Skeletal Radiol* 2012;41:287–292.
13. Otto R, Ferguson MR, Marro K, Grinstead JW, Friedman SD. Limitations of using logarithmic transformation and linear fitting to estimate relaxation rates in iron-loaded liver. *Pediatr Radiol* 2011;41:1259–1265.
14. Abramowitz M, Stegun IA. Handbook of mathematical functions: with formulas, graphs, and mathematical tables. New York: Dover; 1970. xiv, 1046 p.
15. Gudbjartsson H, Patz S. The Rician distribution of noisy MRI data. *Magn Reson Med* 1995;34:910–914.
16. Constantinides CD, Atalar E, McVeigh ER. Signal-to-noise measurements in magnitude images from NMR phased arrays. *Magn Reson Med* 1997;38:852–857.
17. Hamilton JD. Time series analysis. Princeton, NJ: Princeton University Press; 1994. xiv, 799 p.
18. Bonny JM, Zanca M, Boire JY, Veyre A. T_2 maximum likelihood estimation from multiple spin-echo magnitude images. *Magn Reson Med* 1996;36:287–293.
19. Beaumont M, Odame I, Babyn PS, Vidarsson L, Kirby-Allen M, Cheng HL. Accurate liver T_2^* measurement of iron overload: a simulations investigation and in vivo study. *J Magn Reson Imaging* 2009;30:313–320.
20. Hardy PA, Andersen AH. Calculating T_2 in images from a phased array receiver. *Magn Reson Med* 2009;61:962–969.
21. Yin X, Shah S, Katsaggelos AK, Larson AC. Improved R_2^* measurement accuracy with absolute SNR truncation and optimal coil combination. *NMR Biomed* 2010;23:1127–1136.
22. Yu H, Shimakawa A, McKenzie CA, Brodsky E, Brittain JH, Reeder SB. Multiecho water-fat separation and simultaneous R_2^* estimation with multi-frequency fat spectrum modeling. *Magn Reson Med* 2008;60:1122–1134.
23. Berglund J, Kullberg J. Three-dimensional water/fat separation and T_2^* estimation based on whole-image optimization—application in breath-hold liver imaging at 1.5 T. *Magn Reson Med* 2012;67:1684–1693.